Earth and Planetary Science Letters 304 (2011) 168–179

Contents lists available at ScienceDirect

Earth and Planetary Science Letters

journal homepage: www.elsevier.com/locate/epsl

Complex polarity reversals in a geodynamo model

Peter L. Olson [a,*], Gary A. Glatzmaier [b], Robert S. Coe [b]

[a] Department of Earth and Planetary Sciences, Johns Hopkins University, Baltimore, MD 21218, USA
[b] Earth and Planetary Sciences Department, University of California, Santa Cruz, CA 95064, USA

ARTICLE INFO

Article history:
Received 2 September 2010
Received in revised form 26 January 2011
Accepted 29 January 2011
Available online 26 February 2011

Editor: Y. Ricard

Keywords:
geodynamo
polarity reversals
dynamo models
Earth's core
geomagnetic poles

ABSTRACT

Complex polarity reversals in numerical dynamos driven by thermo-chemical convection are analyzed in terms of magnetic field intensity variations, transitional field structure, and other observable characteristics. Our most Earth-like dynamos are characterized by long stable polarity chrons with dipole-dominant magnetic fields punctuated by occasional polarity reversals, and are found within a transition region of parameter space between non-reversing strongly dipolar dynamos and chaotic multi-polar-type dynamos. Dynamos in the transition region have elevated dipole terms, reduced quadrupole terms, magnetic energy that decreases slowly with spherical harmonic degree, and broadband dipole frequency spectra. Their axial dipole intensity histograms are trimodal, with large modes representing the stable polarity states and an intermediate mode representing the transitional multi-polar state. The dipole family intensity exceeds the quadrupole family intensity on the core–mantle boundary during stable polarity times, but during transitions the two families are similar. A complex dynamo model reversal is compared with paleomagnetic reconstructions around the Matuyama–Brunhes polarity transition. Both start with a gradual decrease of the dipole intensity, followed by a precursor reversal and transient polarity recovery, then a rapid dipole collapse and a final reversal that initiates with reverse flux generation in one hemisphere. Virtual geomagnetic poles (VGPs) from sites near the reverse flux trace complex paths and cross the equator several thousand years before the simpler VGP paths from more distant sites, and magnetic intensity variations during the dynamo model reversal correlate with intensity variations inferred for the Matuyama–Brunhes transition.

1. Introduction

Resolving the structure of geomagnetic polarity reversals and excursions is essential to a full understanding of the geodynamo process and for predicting how the Earth system responds to extreme global magnetic field changes. Recent progress toward these objectives has come primarily from two directions: improved resolution of the paleomagnetic field structure before, during, and after reversals and excursions, and a greatly expanded ability to simulate the reversal process using first-principles numerical dynamos and laboratory fluid dynamos.

Thanks to advances in rock magnetic measurement techniques (Channell and Lehman, 1997), radiometric dating (Singer et al., 2005) and expanded geographical coverage (Clement, 2004; Leonhardt et al., 2009; Love and Mazaud, 1997), there are now enough high quality paleomagnetic records of the transition from the reverse polarity Matuyama chron to the present-day normal polarity Brunhes chron around 780 ka to estimate its duration, track VGPs at widely spaced sites, and model the first few spherical harmonics of the surface field prior to and during the event (Ingham and Turner, 2008; Leonhardt and Fabian, 2007).

Following the discovery of spontaneous dynamo reversal by Glatzmaier and Roberts (1995), many hundreds of polarity reversals have been documented in numerical dynamos with widely diverse sets of control parameters. For example, reversals are known to occur in numerical dynamos over a wide range of Ekman numbers, corresponding to very slow rotation (Driscoll and Olson, 2009; Wicht and Olson, 2004; Wicht et al., 2009) moderate rotation (Aubert et al., 2008; Kutzner and Christensen, 2002; Rotvig, 2009) and relatively fast rotation (Takahashi et al., 2005, 2007) rates, and for a variety of thermal and compositional forcing (Glatzmaier et al., 1999; Kutzner and Christensen, 2004; Olson et al., 2010). Comparisons between paleomagnetic records and numerical dynamo reversals often show points of similarity (Amit et al., 2011; Coe et al., 2000; Glatzmaier and Coe, 2007; Olson et al., 2009; Wicht, 2005).

Polarity reversals in numerical dynamos are typically found within a transition region of the physical parameter space, connecting a regime in which dynamos are strongly dipolar, stable, and exhibit relatively small fluctuations and little tendency to reverse, and another regime in which dynamos are highly variable, their field structure is multi-polar, and their dipole component is weak and often highly unstable (Christensen and Aubert, 2006). The stable dipolar regime is characterized by a relatively strong rotational influence

* Corresponding author.
E-mail address: olson@jhu.edu (P.L. Olson).

0012-821X/$ – see front matter © 2011 Elsevier B.V. All rights reserved.
doi:10.1016/j.epsl.2011.01.031

compared to buoyancy effects, and the multi-polar regime is characterized by the reverse situation. Scaling considerations indicate that the Earth's core lies within or close to this transition (Driscoll and Olson, 2009; Olson and Christensen, 2006), suggesting that the geomagnetic reversal phenomena is linked to the ability of the geodynamo, which spends most of the time in a stable dipolar state, to occasionally access a less stable multi-polar regime, possibly through random internal fluctuations. It has been argued that this transition region is characterized by a specific range of values of a local Rossby number parameter (Christensen and Aubert, 2006; Wicht et al., 2009) which measures the ratio of inertial to Coriolis effects in the outer core fluid motions, with local Rossby numbers greater than about 0.2 corresponding to the multi-polar regime and values smaller than about 0.05 corresponding to the stable dipolar regime. It has also been argued that geodynamo states with more frequent reversals are marked by relatively lower levels of equatorial anti-symmetry of the field with the axial dipole term removed (Coe and Glatzmaier, 2006).

Spontaneous polarity reversals have also been observed in laboratory fluid dynamo experiments. In the VKS (von Karman sodium) experiment, a turbulent swirling flow is generated in liquid sodium between two coaxial counter-rotating impellers within a cylindrical container (Monchaux et al., 2007). A variety of induced magnetic field regimes have been observed in the VKS experiment as a function of the individual impellers magnetic Reynolds numbers, including a regime with irregularly-spaced polarity reversals that also includes shorter events suggestive of polarity excursions (Berhanu et al., 2007). Like the reversals in numerical dynamos, the VKS reversals are observed to occur within a narrow range of parameters, when the magnetic Reynolds numbers of the impellers are in the ranges of 42 ± 2 and 32 ± 4, approximately. Individual VKS reversal records show a remarkable degree of repeatability, including dipole collapse, rapid polarity change, and fast dipole intensity recovery stages (Berhanu et al., 2007). Polarity reversals are also seen in laboratory fluid dynamos that use external amplification. A laboratory dynamo of the Bullard–von Karman (BVK) type consisting of twin impellers driving a turbulent vortex in liquid gallium with an external current amplifier also produces reversals, and in this experiment the reversals show clustering and other long time scale statistical correlations (Sorriso-Valvo et al., 2009). Neither the VKS nor the BVK reversals show complexity or much evidence of a multipolar transitional field state, perhaps because these experimental dynamos are typically more turbulent and have relatively less rotational influence compared to reversing numerical dynamos.

If we suppose that geomagnetic reversals occur because the geodynamo lies in a transition region and is subject to symmetry breakdown, then we expect the transition from the stable dipole-dominated field structure to the less stable, lower symmetry multipole field structure to be a part of the reversal process. During such reversals there may be precursors in which the field reverses one or more times, and in addition, the multi-polar stage may persist for a substantial time. Following Coe and Glen (2004), we use the term “complex reversals” to characterize polarity changes that include precursory events, substantial multi-polar stages, and produce highly diverse virtual geomagnetic pole (VGP) records at different sites. Another consequence of the geodynamo lying within this transition region is that it will sometimes access the multi-polar state but fail to produce a reversal. If the axial dipole field happens to be in its original polarity at the end of the multi-polar stage, then the geodynamo will simply return to its original dipolar state without fully reversing. This general scenario has been used to describe polarity excursions in the paleomagnetic record (Gubbins, 1999; Valet et al., 2008), which appear to be very short-lived, possibly lasting only a few thousand years.

Paleomagnetic evidence indicates that the most recent polarity reversal at the 780 ka Matuyama–Brunhes transition (hereafter denoted by MBT) was preceded by major changes in the geomagnetic field structure, including a precursor and a possible multi-polar field state, and accordingly, may have been a complex reversal. Global paleointensity reconstructions reveal that long before the MBT, the geomagnetic field intensity decreased by a factor 2–3 through a sequence of steps, each step lasting about 15 kyr (Valet et al., 2005). Events preceding and during the MBT have been examined in more detail using high-precision dating, high-resolution deep sea sediment records and also global reconstructions in which the paleomagnetic field structure is represented using low degree spherical harmonics, including dipole, quadrupole, octupole, and in some cases hexadecupole terms (e.g. Leonhardt and Fabian, 2007). Dates of transitional lavas show two clusters, one around 780 ka, and the other around 795 ka (Singer et al., 2005); the earlier cluster date being proposed as a precursor to the actual reversal (Hartl and Tauxe, 1996). The actual reversal is characterized by very complex transitional VGP paths, according to high-resolution Ocean DrillingProgram records (Channell and Lehman, 1997), which include multiple swings across the equator with large excursions in the VGP longitude. This differs from the simpler behavior seen in other records, which show more north–south VGP paths and sometimes a tendency for transitional VGPs to concentrate in preferred longitude bands (Clement, 1991) or isolated patches (Hoffman, 1992).

A 40 kyr global intensity reconstruction by Ingham and Turner (2008) spanning the MBT includes a 20 kyr long precursor stage in which the normally weak non-dipole field exceeds the dipole field intensity at the Earth's surface, consistent with a multi-polar field at the core–mantle boundary (CMB) during that time. This is followed in their reconstruction by a stage when the dipole intensity partially recovers and briefly exceeds the surface non-dipole intensity, which in turn is followed by a very rapid dipole intensity collapse, final reversal, and recovery of the dipole intensity in the new polarity, all of which occur within about 5 kyr. Another paleomagnetic reconstruction by Leonhardt and Fabian (2007) spans 20 kyr around the MBT and shows basically the same sequence of intensity variations in the 5 kyr around the reversal. Their reconstruction starts at 785 ka, approximately 11 kyr before the dipole minimum and therefore does not resolve all of the precursory behavior reported by Ingham and Turner (2008). Nevertheless, as Amit et al. (2011) have demonstrated, the Leonhardt and Fabian (2007) reconstruction does show precursory effects, including dipole decrease and collapse stages, and it also shows evidence of complexity, in which the reversal ages – the age at which the VGP crosses the equator – are several thousand years older from sites in the northern hemisphere compared to similarly-defined ages from sites in the southern hemisphere.

In this paper we show that some polarity reversals in numerical dynamos driven by thermal and compositional convection with coupling between core heat loss and inner core growth involve the complex effects just described. We analyze one reversal in detail, showing how the field structure and symmetry change over a wide spectrum of time scales before and during the reversal. We also show that this complex model reversal exhibits many of the characteristics of the Leonhardt and Fabian (2007)and other paleomagnetic reconstructions around the MBT.

2. Dynamo model and parameters

The numerical dynamo is similar to that described in Glatzmaier and Roberts (1996). It solves the compressible Navier–Stokes equation with full inertial terms, the magnetic induction equation, and separate equations for the transport of heat and light elements in a rotating sphere using the anelastic approximation. We chose a numerical resolution to allow for long time simulation, with maximum angular resolution corresponding to a rhomboidal truncation of spherical harmonics with degrees up to $l_{max} = 95$ and orders up to $m_{max} = 47$, and 49 Chebyshev levels in radius.

The model Ekman number is defined as

$$E = \frac{\nu}{d^2\Omega} \tag{1}$$

where ν, d, and Ω are outer core viscosity, thickness, and angular velocity of rotation, respectively. Our model Rayleigh number is defined as

$$Ra = \frac{4g\beta d^4}{\kappa_T \nu}\frac{dS}{dr} \tag{2}$$

where g, $\beta = 1/\rho\partial\rho/\partial S$, dS/dr, ρ and κ_T are gravitational acceleration, rate of change of density with entropy at constant composition, entropy gradient, density, and thermal diffusivity, respectively, all evaluated in the outer core at the CMB. The factor of 4 in Eq. (2) converts the thermal Rayleigh number to a total Rayleigh number, since the production rate of compositional buoyancy at the inner core boundary (ICB) is set to be three times larger than the thermal buoyancy. Other control parameters include the Prandtl number, the Lewis number, and the magnetic Prandtl number, which are

$$Pr = \frac{\nu}{\kappa_T}, \tag{3}$$

$$Le = \frac{\kappa_\xi}{\kappa_T} \tag{4}$$

and

$$Pm = \frac{\nu}{\eta}, \tag{5}$$

respectively, where κ_ξ is compositional diffusivity and η is magnetic diffusivity. In all our dynamos $Pr = Le = 1$. Separate equations and boundary conditions are used for the transport and diffusion of both entropy and composition. The viscous, thermal, and compositional diffusivities are all assumed to be turbulent and set to 20 m^2/s; the magnetic diffusivity is set to a nominal Earth's core value $\eta = 2$ m^2/s. No hyperdiffusion is employed. All radially-dependent variables, specifically the gravitational acceleration, density, temperature, pressure, and thermodynamic derivatives are based on the Earth model PREM.

A spatially uniform heat flow at the CMB is prescribed in all cases. In contrast to the usual co-density formulation for thermo-chemical convection in the core (Driscoll and Olson, 2009; Olson et al., 2010), our model uses an ICB condition that couples the release of sensible and latent heat and the light element fluxes to the local time rates of change of the entropy and the composition on the ICB (see Braginsky and Roberts, 1995; Glatzmaier and Roberts, 1996). The solid inner core and the mantle are free to rotate according to the magnetic and viscous torques on them. The electrical conductivity of the inner core is constant and the same as the fluid outer core. For the mantle, a finite electrical conductivity is prescribed in a thin layer just above the CMB, with a total conductance of 4×10^6 S, equivalent to the conductivity of the core distributed over a depth of 10 m. This layer provides for a weak electromagnetic couple with the outer core.

A spectral method is employed to solve the system of equations, using a poloidal–toroidal decomposition for the mass flux and magnetic field vectors (Glatzmaier, 1984). All variables are expanded in spherical harmonics to resolve their horizontal dependencies and in Chebyshev polynomials to resolve their radial dependencies. Linear terms are treated implicitly; nonlinear terms are treated explicitly using a spectral transform method.

The various dynamo cases correspond to different rotation rates (i.e., E) and different prescribed heat flows at the CMB (i.e., Ra). Our total Rayleigh number is in the range $Ra = 0.6 - 1.9 \times 10^6$, roughly 5–20 times critical for our Ekman numbers, which range from $E = 0.5$– 1.0×10^{-3}.

Table 1
Dynamo cases summary. E = Ekman number; Ra = Rayleigh number; Myr = run duration in Myr; Dp = average dipolarity, the ratio of dipole to total magnetic field intensity on the CMB; types = dominant field type: D = dipolar, and M = multi-polar. Parentheses indicate subordinate field dipolarity and type.

Case	E ($\times 10^{-3}$)	Ra ($\times 10^6$)	Myr	Dp	Types
a	1.0	0.62	2.3	0.45	D
b	1.0	1.24	2.4	0.35(0.2)	D(M)
c	1.0	1.86	1.3	0.15	M
d	1.0	1.55	1.0	0.2(0.35)	M(D)
e	1.0	0.94	2.0	0.4(0.2)	D(M)
f	1.0	1.39	1.9	0.31(0.2)	D(M)
g	0.5	1.24	0.7	0.52	D
h	0.8	1.24	1.5	0.45	D
i	0.9	1.24	1.4	0.38(0.15)	D(M)

The maximum amplitudes of the resulting fluid velocities and internal magnetic fields are typically a few 10^{-3} m/s and a few gauss, respectively, and the rms fluid velocity is about 3×10^{-4} m/s. Because a relatively large Ekman number and small Rayleigh number are necessary for long simulation times, our rotation periods are about 10^4 times too long and our CMB heat flows are about 10^4 times too small, relative to Earth values. Even so, the convection in these models is strongly influenced by the rotation. Typical values for the Rossby number, the ratio of inertia to Coriolis acceleration, are 0.02 based on the outer core depth d, and 0.1 based on the typical cross sectional dimension of a convection column. We note that this later value is very close to what Christensen and Aubert (2006) and Olson and Christensen (2006) found for the transition from dipolar to non-dipolar dynamos.

3. Results

Table 1 summarizes the 9 dynamo cases used in this study in terms of their Ekman number E, the thermo-chemical Rayleigh number Ra, the run duration in Myr based on an assumed 20 kyr free decay time scale for the dipole field, the dipolarity Dp and the type of dynamo, with D = dipole dominant and M = multi-polar. Here, dipolarity is defined as the ratio of rms dipole intensity to rms total field intensity on the CMB. For dynamos in the transition region, the first entry in the last two columns of Table 1 refers to the predominant behavior and the second entry in parentheses refers to the subordinate behavior.

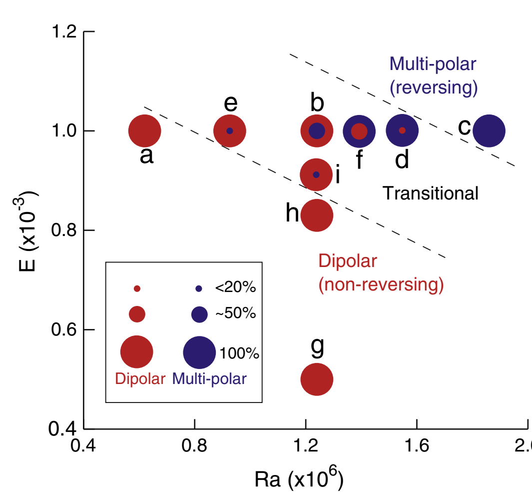

Fig. 1. Dynamo regimes for dipolar and multi-polar magnetic field states as a function of Ekman number E and Rayleigh number Ra. Cases a–i from Table 1 are labeled. Insert shows the approximate time fraction in each state. Dynamos in the transitional region have the most Earth-like field structure and reversal behavior, including complex reversals.

Fig. 1 is a regime plot of the dynamos in Table 1, showing the systematic trends as a function of the Rayleigh number and the Ekman number. The circle diameters denote the approximate relative proportions of time spent in dipolar and multi-polar states during the simulation. Cases labeled a, d, and i are discussed below. The two main regimes in Fig. 1 are the stable (non-reversing) dipolar regime in the lower left portion of the plot (corresponding to the combination of low *Ra* and low *E*) and the highly variable, reversing multi-polar regime in the upper right (corresponding to the combination of high *Ra* and high *E*). The approximate boundaries of the transitional region between the two main regimes are shown by dotted lines. Within the transitional region, the relative proportions of time spent in the dipole dominant and multi-polar states are indicated by the change in the relative sizes of the shaded circles. The trend with increasing *Ra* or *E* in the transition region is from mostly dipolar dynamos with infrequent multi-polar episodes that occasionally reverse polarity, toward mostly multi-polar dynamos with infrequent dipolar episodes that reverse frequently. Because the trends in this region indicate a continuous variation from dipolar to multi-polar structure, it is better described as a transition region where both dipolar and multi-polar field structures are present at various times in a single dynamo, as opposed to a discontinuity that separates the two main regimes.

Fig. 2 summarizes the behavior of the dynamos in the non-reversing dipolar and multi-polar regimes and in the transition region. Columns from left to right in Fig. 2 show the dynamo case and type as defined in Table 1 and Fig. 1, the distribution of the dipole axis locations, histograms of the rms axial dipole field intensity on the CMB with the sign preserved, the time averaged power spectrum on the CMB as a function of the harmonic degree *l*, and the frequency spectra of the dipole and axial dipole fluctuations. No scaling factors have been applied to the magnetic field intensities in this or any of the subsequent figures; we note that the typical field intensities produced by these models (without scaling applied) are weaker than the present-day geomagnetic field intensities by slightly more than one order of magnitude.

Case a is clearly in the non-reversing dipole regime. Nearly all of its dipole axis locations lie within 20° of the north pole and show an isotropic distribution about the rotation axis. The dipole field has quite high intensity but low variability in this case, as indicated by the shape of its axial dipole intensity histogram. Over the entire 2.3 Myr

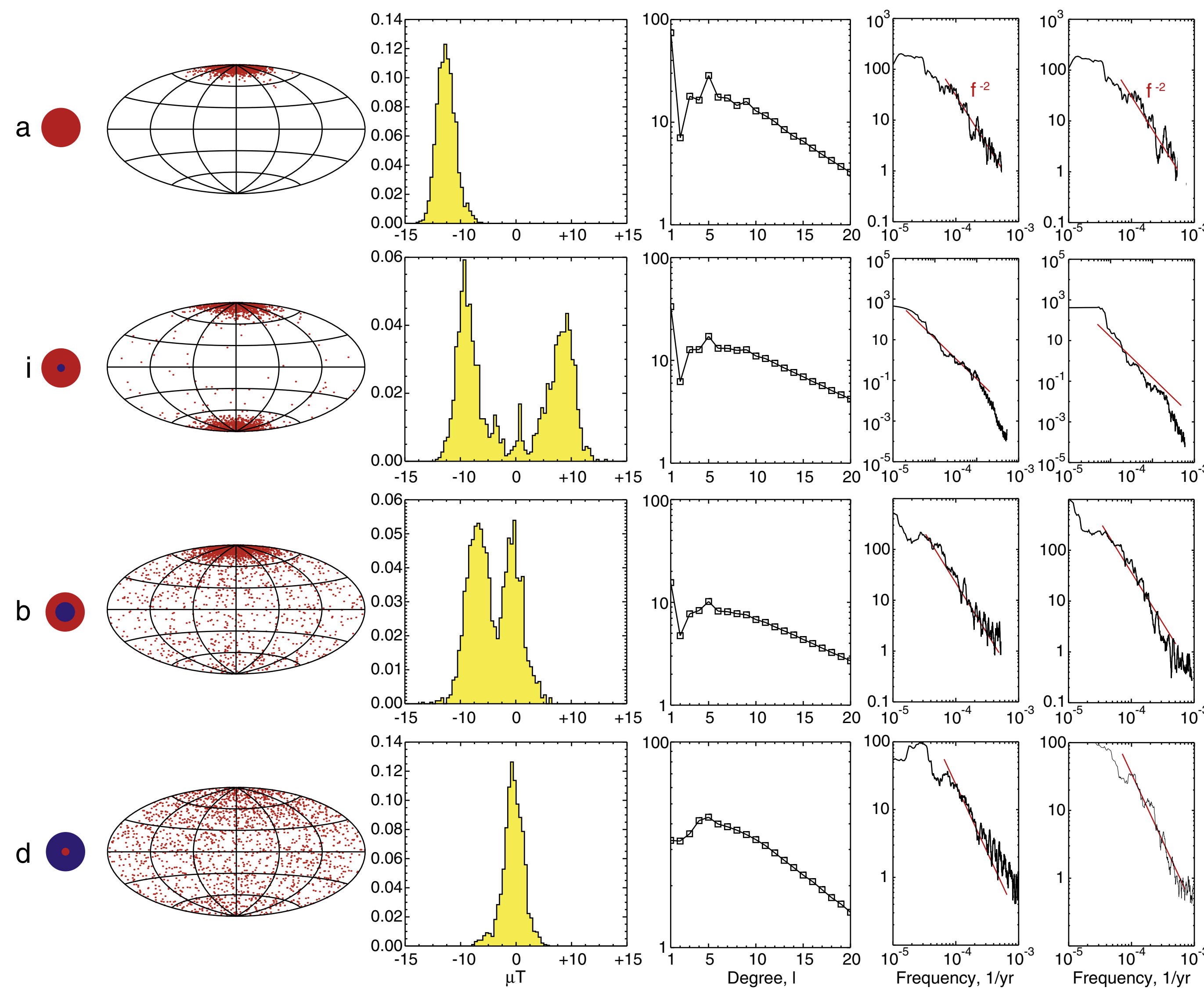

Fig. 2. Summary of dynamo behavior. Columns from left to right: dynamo case as defined in Table 1, dynamo type with symbols as defined in Fig. 1; geomagnetic pole locations; CMB axial dipole intensity histograms in microtesla; time averaged CMB power spectra in squared microtesla as a function of spherical harmonic degree *l*; dipole frequency spectra (unsmoothed) with f^{-2} reference lines; and axial dipole frequency spectra (unsmoothed) with f^{-2} reference lines.

simulation time, the dipole intensity failed to drop to the weak intensities that characterize the dynamos in the multi-polar regime. The power spectrum of this case shows a strong alternation between odd and even terms at low spherical harmonic degrees, especially the highly elevated dipole and deeply suppressed quadrupole terms. The power spectrum decays exponentially at higher degrees. The energy in its dipole and axial dipole frequency spectra is broad-band, lacks significant peaks, and falls off at higher frequencies like f^{-2}, approximately.

In contrast, Case d lies within the transition region but close to the multi-polar regime. Its dipole axis locations are nearly evenly distributed over the sphere, with only a slight bias toward polar locations. The axial dipole intensity histogram in Case d is also quite narrow, but its mean value and its mode (most frequent value) are both very close to zero. Interestingly, the shape of the histogram of multi-polar Case d is practically the same as the shape of the histogram of non-reversing Case a with an x-axis reflection and shift applied. However, there are large differences in their respective CMB power spectra. Whereas Case a is dipole dominant, the power spectrum of Case d peaks at harmonic degree $l=5$, and the power in the dipole (degree $l=1$) is less than all harmonics up to about degree $l=10$. Case b is roughly midway between Cases a and d in that the dipole and multi-pole states occupy about one half of the simulation time. Although this case transitioned from the dipole to the multi-pole structure four times, none of these transitions produced a long-lasting stable reversed dipole (two reversed dipole states were recorded, but these were short-lived and barely appear in the pole locations or intensity histograms for Case b in Fig. 2). The absence of a stable reversal in this case is possibly a statistical artifact of the finite simulation time. Alternatively it may indicate a long-lived polarity bias, an effect which has been reported in other numerical dynamos (Wicht et al., 2009).

Case i is also intermediate between Cases a and d, and in several important respects it is more Earth-like than the others. It lies within the transition region of Fig. 1 but close to the non-reversing regime, and therefore is characterized by relatively long stable dipolar chrons and widely separated polarity events. Its dipole axis locations have nearly as much polar concentration as Case a, but in Case i both polarity states are represented in nearly equal portions. In addition there is a scattering of low latitude pole locations representing polarity events, including transitional locations with a large distribution of longitudes and latitudes, but little indication of clustering. The axial dipole intensity histogram is trimodal in this case, with two large peaks representing the dipolar stable polarities and a smaller central peak representing the multi-polar transitional state. Note that the peak dipole intensities of the stable states are weaker in the occasionally reversing Case i than the non-reversing Case a. In addition, the three peaks in the Case i histogram show finite overlap, which reflects the ability of this dynamo to transition from one mode to the next. In terms of its shape, the power spectrum of Case i is also the most Earth-like in Fig. 2. It shows dipole dominance and quadrupole suppression, with essentially flat behavior between degrees $l=3$ and 9 except for a slightly elevated $l=5$ term that represents the peak in the kinetic energy spectrum. At higher degrees the spectrum decays exponentially but with a small exponential factor, like the geomagnetic spectrum. The dipole frequency spectrum of Case i approximately follows an f^{-2} trend below $f=10^{-3}\,\mathrm{yr}^{-1}$, then decays faster at higher frequencies, approximately like $f^{-11/3}$.

Fig. 3 shows 0.85 Myr long time series records of the main field structure from Case i, including the stages before, during, and after a polarity change between two stable dipolar states. The top panel shows the time series of the axial dipole rms intensity on the CMB, the lower panel shows the time series of the rms intensity of the field on the CMB for the dipole and quadrupole families, respectively. The shaded region marks the complex polarity transition. In terms of the decay, reversal and re-saturation of the axial dipole moment, the entire reversal process lasts about 100 kyr in this case. In comparison, Valet et al. (2005) find ~50 kyr for the peak-to-peak intensity variation around the MBT and ~100 kyr for the peak-to-peak intensity variation around the Upper Jaramillo event. It should be noted that our model times are calculated on the basis of an Earth-like magnetic diffusion time, rather than the convective overturn time or the rotation period, both of which are too long in our model compared to Earth values.

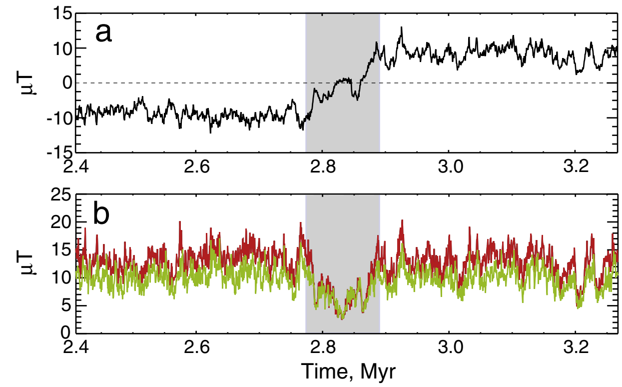

Fig. 3. Low resolution time series from dynamo Case i. a: CMB axial dipole intensity (rms) b: CMB magnetic field intensity (rms); red = dipole (odd) family, and green = quadrupole (even) family.

During the stable polarity chrons before and after the reversal, the dipole family intensity consistently exceeds that of the quadrupole family, and the two families fluctuate in phase. But starting with the first major collapse of the axial dipole around $t=2.78$ Myr, the intensities of the two families become comparable, although their fluctuations remain closely synchronized in time and the amplitudes and shapes of the fluctuations during the transition are essentially the same as during the stable polarity times. In essence, the primary difference in the main field symmetry between transitional and stable polarity times in Fig. 3 is the much-reduced intensity of the dipole family and a somewhat smaller reduction of the quadrupole family during the transition.

The time resolution in Fig. 3 is too coarse to show all the stages of the reversal process. Fig. 4 shows the expanded (medium resolution) time series of the Case i reversal, spanning approximately 100 kyr, the time represented by the shaded region of Fig. 3. The top panel a in Fig. 4 shows rms magnetic field intensities on the CMB, including the total field in blue, the dipole (odd) family in red, and the quadrupole (even) family in green. The second panel b shows the rms dipole intensity on the CMB. The third panel c shows the energy in the dipole field and the non-dipole field extrapolated to the Earth's surface, and the bottom panel d shows the dipole latitude. Bars labeled 1–8 in Fig. 4 indicate the image times in Fig. 5.

The initial dipole collapse begins around time $t=2.78$ Myr in Fig. 4, nearly 80 kyr before the final directional transition occurs. The dipole energy drops by a factor of 50 within about 7 kyr, then slowly begins to strengthen over the next 12 kyr, recovering about one half of its pre-collapse intensity, before continuing a stepwise, cascading decrease. Prior to $t=2.815$ Myr the dipole latitude is mostly confined to within 15° of the pole, the dipole energy equals or exceeds the non-dipole energy at the surface, and the dipole family exceeds the quadrupole family on the CMB, so that in spite of the ongoing dipole collapse, the field retains most of its stable chron properties. This is reflected in the images of the dynamo interior shown in panels 1 and 2 of Fig. 5, which show that the internal structure is overwhelmingly dominated by the normal polarity magnetic flux at these times. Starting around $t=2.820$ Myr, however, Fig. 4 shows that the quadrupole family intensity surpasses the dipole family intensity on the CMB, the non-dipole energy matches the dipole energy at the

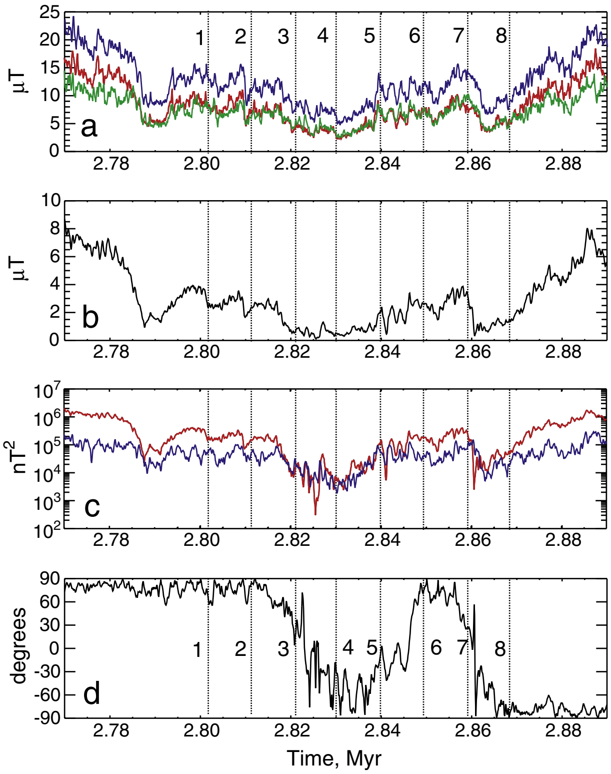

Fig. 4. Medium resolution time series from dynamo Case i. a: CMB magnetic field intensity (rms); blue = total field, red = dipole (odd) family, and green = quadrupole (even) family; b: CMB dipole field intensity (rms); c: energy (mean squared field intensity) on the Earth's surface; red = dipole and blue = non-dipole. d: dipole latitude. Dotted lines labeled 1–8 denote image times in Fig. 5.

surface, and the dipole latitude goes unstable and swings into the southern hemisphere. These precursory events are reflected in panels 3, 4, and 5 of Fig. 5, which show that the internal field structure at these times is a mixture of the two polarities.

Instead of completing the reversal process, the dynamo briefly recovers its original polarity with a somewhat strengthened dipole field between $t = 2.845$ and 2.860 Myr. The dipole axis returns to positions near the north pole and for a short time the dipole energy exceeds the non-dipole energy at the surface. Once again, these events are reflected in the dynamo interior by a return to predominantly normal polarity magnetic flux in panels 6 and 7 of Fig. 5. Had the instability been quenched at this stage, the preceding events would be seen at the surface as a transient, although somewhat long-lasting dipole field excursion. The reversal process was not quenched, however. The final dipole collapse begins around $t = 2.860$ Myr, and precipitates a rapid dipole directional transition as the dipole axis crosses the equator a second time, moving nearly 130° in less than a thousand years. The new reversed polarity is established over the next few thousand years, so by $t = 2.865$ Myr the internal field is nearly all reversed, as shown in panel 8 of Fig. 5. Thereafter, the dipole and non-dipole fields recover toward their stable chron levels, with the former growing at a faster rate than the later, completing the reversal process.

Consistent with previous dynamo reversal studies (Aubert et al., 2008; Wicht and Olson, 2004), the reversal process inside the core is primarily a magnetic field instability, and only secondarily an instability or transition in the structure of the convective flow. There appears to be some perturbation to the flow field, particularly evident in panel 7 of Fig. 5 just as the final dipole collapse and rapid directional change occur, where the columnar-style convection that dominates the stable chrons appears to break up throughout large parts of the outer core, returning only when the new magnetic polarity takes over. However, the images in Fig. 5 demonstrate that the flow field is continuously fluctuating, even with stable polarity, and the fluctuations that accompany the polarity change are not appreciably larger than the velocity fluctuations at other times.

Because of its extreme rapidity, the final dipole collapse and field directional change are not well-resolved in the time slices of Fig. 5, and their internal origin cannot be seen. Fig. 6 shows in expanded form the detailed time series of the final stage of the polarity reversal in Case i, spanning only 20 kyr. The upper panel (a) shows the time variation of the ratio of the even/odd family field intensities on the CMB (solid) and dipole axis latitude (dots). The middle panel (b) shows the time variation of the dipole (solid) and non-dipole (dashed) magnetic energies at the surface. Note the transient strengthening of the dipole and non-dipole fields as well as the even/odd field intensity ratio, which reaches a maximum of 1.5 about 1 kyr prior to the directional change. This zoomed record demonstrates how rapidly the main directional change occurs when the dipole field is weak; the dipole latitude changes by 130° in about 400 years. Also note that the dipole field energy remains slightly above the non-dipole energy until the actual directional change, when it falls below the non-dipole energy for about 1 kyr. In addition, the energy in both the dipole field and the non-dipole surface fields remain quite low for several thousand years after the main directional change.

Panel c in Fig. 6 shows the MBT dipole and non-dipole surface energies according to the Leonhardt and Fabian (2007) reconstruction, plotted on the same time scale as our model surface energies. The correspondence between model energies and the reconstructed MBT energies is rather good. Over the 20 kyr period, the correlations between model and reconstructed MBT dipole and non-dipole energies are 0.82 and 0.75, respectively. In addition, the same sequence of events are evident in both the dynamo model and the reconstructed reversal. To be sure, we have exercised selectivity in choosing dynamo Case i for comparison, and it is true that not every complex model reversal corresponds so closely to the MBT reconstructions. Nevertheless, it is significant that the dynamo models in the transition region produce complex reversals as well as simpler ones, and both of these reversal types have properties in common with paleomagnetic reversals.

There are other similarities between our model reversal and the Leonhardt and Fabian (2007) MBT reconstruction. Fig. 7 shows the VGP paths at sites located along 45 N and 45 S latitudes during the precursor reversal, and Fig. 8 shows the VGP paths at selected sites during the transient polarity recovery and the final reversal. The absolute longitudes of the sites in these figures are arbitrary with respect to the dynamo model longitudes (the continents are shown for reference purposes only), but their distribution serves to illustrate how the transitional VGPs depend on the location of the site with respect to the origin of the reversal. The end-stage directional changes are highlighted using arrows and dark colored paths.

The most systematic effect in Figs. 7 and 8 is the difference between VGP paths at northern hemisphere versus southern hemisphere sites during the precursor reversal and during the final reversal. Comparing the VGP paths in Fig. 7a and b, it is clear that the precursor reversal originates in the southern hemisphere. Large amplitude deviations from normal polarity occur first at the four southern sites and the VGP reaches high southern latitudes at three of these sites within the time span shown. One southern site has multiple VGP latitude swings, and another site has VGPs that are basically transitional throughout the time interval. In contrast, the VGPs in Fig. 7a barely deviate from normal polarity at three of the northern sites and only temporarily stray across the equator at the fourth northern site.

Fig. 8 shows that there are systematic differences between VGP paths in the northern and southern hemispheres for the final

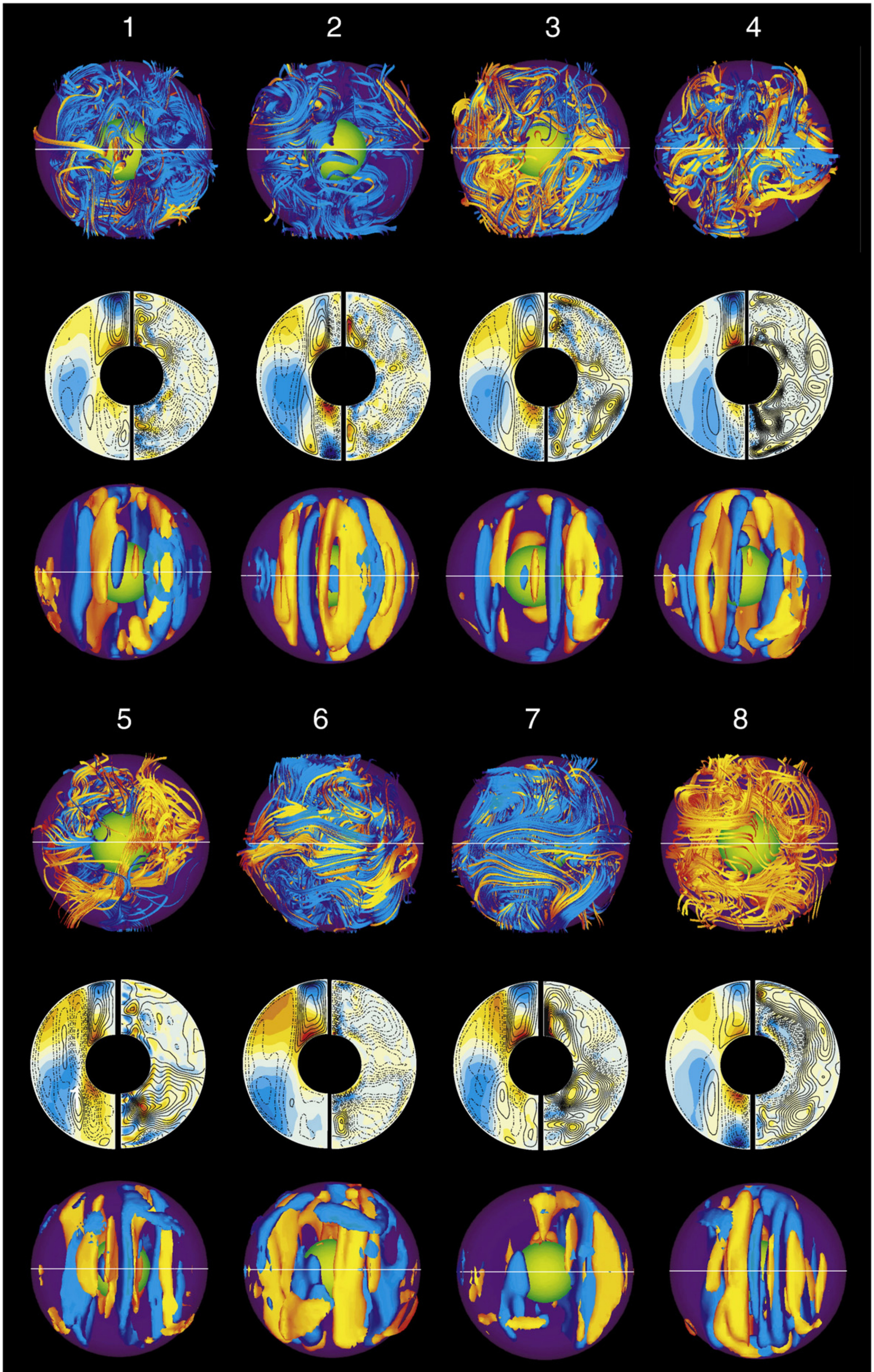
1
2
3
4
5
6
7
8

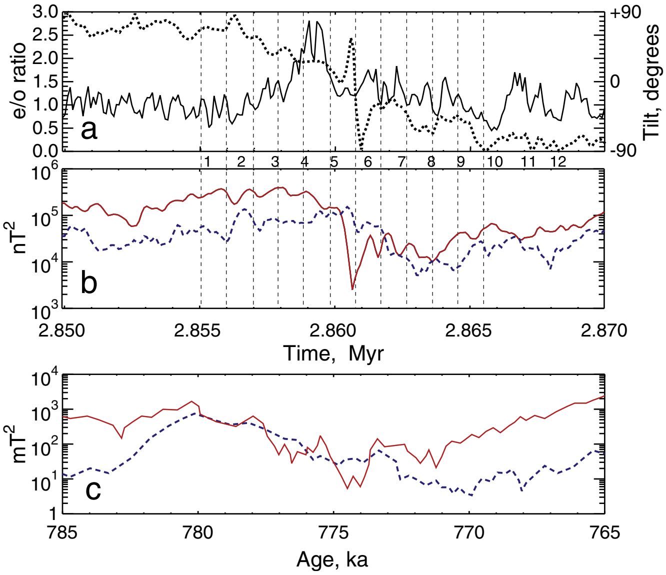

Fig. 6. High resolution time series of the final polarity reversal in dynamo Case i. a: Time series of the even/odd family magnetic field intensities at the surface with the axial dipole removed (solid) and dipole axis latitude (dots); b: time series of surface dipole (solid) and non-dipole (dashed) magnetic energies; c: time series of surface dipole (solid) and non-dipole (dashed) magnetic energies from a 20 kyr reconstruction around the Matuyama–Brunhes polarity transition by Leonhardt and Fabian (2007) plotted with the same time scale.

reversal, which are not evident for the transient polarity recovery event. Fig. 8a shows the paths from sites at 45 N and 43 S starting at 2.84449 Myr and lasting 5.6 kyr, including the polarity recovery. Fig. 8b shows the paths from sites at 45 N and 43 S starting at 2.85485 Myr and lasting 8 kyr including the final polarity reversal. VGPs are plotted 95 years apart and the large, late-stage directional changes are highlighted with arrows and darker paths. At the southern sites in Fig. 8b the VGP paths cross the equator early in the record and show relatively large amounts of east–west looping, whereas the VGP paths at the northern sites are relatively confined in latitude and cross the equator later in time. The difference in the reversal time between northern and southern sites, measured by the times at which the VGP paths cross the equator, is about 2800 years for the final reversal in Fig. 8b.

The reason for the systematic differences between hemispheres is that the precursor and final reversals originate mainly in the southern hemisphere of the dynamo model. Fig. 9 shows the snapshots of the radial component of the magnetic field B_r on the model CMB at the twelve times labeled in Fig. 6. At snapshot 1 the CMB field is dominated by high latitude normal polarity flux spots, particularly strong in the northern hemisphere, with high latitude normal polarity VGPs at all sites in Fig. 8b and a small e/o field ratio in Fig. 6. At snapshot 2, reverse flux spots appear at mid latitudes in the south, increasing their strength at snapshot 3 and decreasing the e/o field ratio. This time corresponds to the first destabilization of the VGP at the south Atlantic site in Fig. 8b, which happens to be the site closest to the reverse flux. The southern reverse flux spot strengthens and moves poleward at snapshot 5, while the old normal polarity flux spots in the southern hemisphere migrate toward the equator during snapshots 5–7, resulting in a non-axial quadrupole dominated field at the end of this sequence. This sequence corresponds to the rapid dipole collapse in Fig. 6, the major directional changes at the southern sites and the VGP looping at the northern sites in Fig. 8b. The biggest northern VGP directional changes in Fig. 8b correspond to snapshots 8 and 9 in Fig. 9, when the CMB field is multipolar, nearly three thousand years after the directional changes at the southern sites. During snapshots 11 and 12 the reverse polarity dipole is strengthening, while the e/o ratio in Fig. 6 increases and the VGPs are at high southern latitudes at all sites.

The observation that reverse magnetic flux emerges from the dynamo interior first in the south and several thousand years later in the north suggests that transport of reverse flux across the equator by the meridional circulation may play a role in this reversal, as was found previously by Wicht and Olson (2004). Fig. 5 shows that the circulation in Case i includes south to north meridional velocity beneath the CMB, with a speed of about 5×10^{-5} m/s. This speed corresponds to 90° of frozen flux transport in about 3 kyr, which is comparable to the time difference between the VGP equator crossings at northern versus southern sites in Figs. 7 and 8.

Because the southern hemisphere sites are much closer to the strong reverse flux patches that initiate the reversals, during the polarity changes the transitional magnetic field at these sites is less dipolar than the field at sites in the northern hemisphere. There is also a strong azimuthal circulation in the southern hemisphere of the outer core during the reversal events that produce strong westward magnetic drift, so the VGP tends to move in longitude at the southern sites. The northern sites in Figs. 7 and 8 are farther from where the reversals originate, so they see mostly the smoother advected field and record simpler, more longitudinally confined VGP paths that cross the equator later in time, both for the precursor and final polarity events. Such differences are not evident in the VGP paths during the polarity recovery event shown in Fig. 8a. For this event the initial and final VGP locations are coherent at all sites, and the main equator-crossing portion of each path is contemporaneous at three of the four sites. Fig. 4 shows that the dipole field is stronger during the polarity recovery event compared to the precursor and final reversals, which offers an explanation for why its VGP paths are more north–south and more coherent between sites.

Interestingly, the northern sites show some tendency for transitional VGP clustering during both the precursor and the final reversal, a behavior that has been seen in paleomagnetic reversals and has been attributed to the effects of mantle heterogeneity (see Hoffman, 1992, 1996). Although mantle heterogeneity is not a property of this particular dynamo model, there are times during the reversal when the transitional field structure is relatively stable, and the VGP clusters seen in Figs. 7 and 8 correspond to those times. For example, the VGP clusters at the northern sites in Fig. 8b reflect the comparable dipole and quadrupole contributions to the transitional field structure seen in snapshots 6 and 7 of Fig. 9.

The southern VGP paths in Figs. 7 and 8b have features in common with those reported by Channell and Lehman (1997) for the MBT recorded in rapidly deposited sediment from the northern Atlantic, which feature multiple equator crossings and multiple east–west VGP swings that cover nearly all longitudes. This behavior is in marked contrast to the many simpler MBT records from other sites, which show more unidirectional, north–south VGP motion. One explanation for this seeming paradox is that many of the relatively simple transition VGP records may have been heavily smoothed by their recording processes, and that the actual complexity of the MBT is evident only in the higher fidelity records with less smoothing (see Coe and Glen, 2004). For nearby sites with simpler transition records, such as DSDP Hole 609B (Clement and Kent, 1987) only 1200 km to

Fig. 5. Snapshots of internal structure during polarity reversal in dynamo Case i. First and fourth rows: internal magnetic field lines colored by sign of the axial field in the equatorial plane (red/yellow = positive; blue = negative); Second and fifth rows: contours of zonal average structure; left = azimuthal velocity in colors with meridional streamlines; right = azimuthal current in colors with poloidal magnetic field lines; third and sixth rows: axial vorticity (red/yellow = positive; blue = negative). Numbers correspond to time slices in the time series Fig. 4.

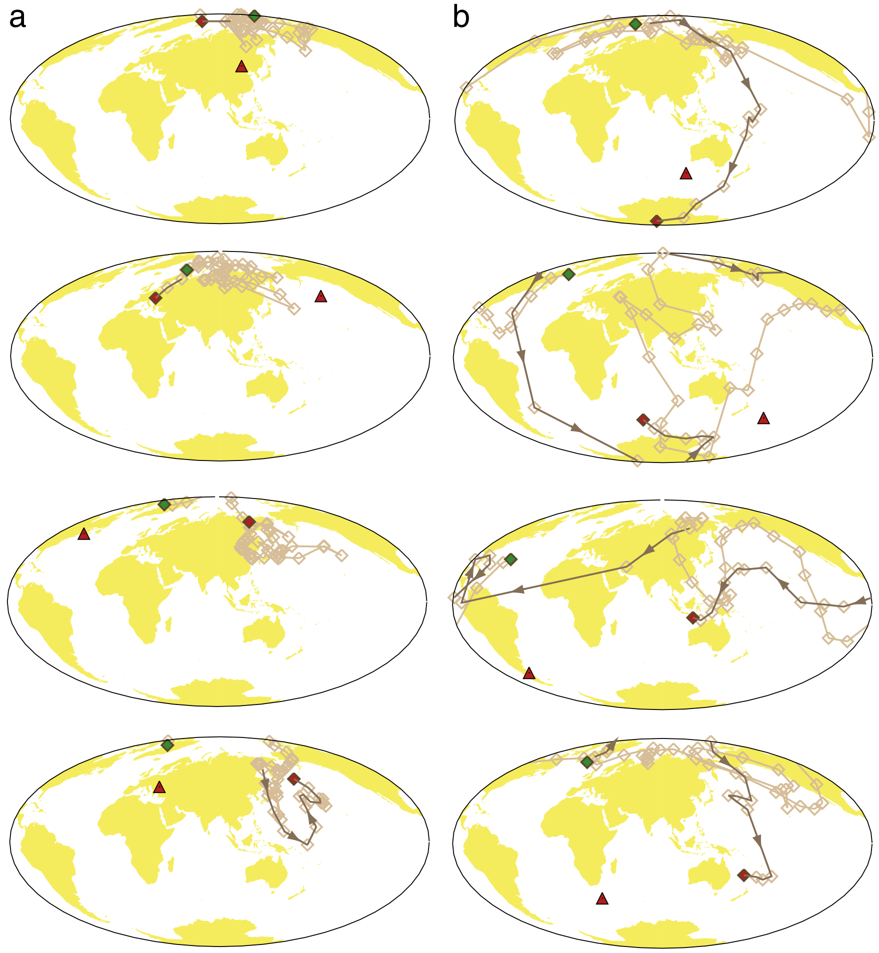

Fig. 7. Virtual geomagnetic pole (VGP) paths at sample locations starting at 2.81682 Myr including the precursory reversal in dynamo Case i. Left column (a) shows paths from sites at 45 N; right column (b) shows paths from sites at 45 S. Continental outlines are shown for reference only, as the absolute longitudes are arbitrary. Data points are 95 years apart and the paths are 4.81 kyr long. Large, late-stage directional changes are shown with arrows and darker paths. Site locations are marked by triangles; first and last VGPs are colored in green and red, respectively.

the south, smoothing is a viable explanation, assuming the complexity of the Channell and Lehman (1997) records is real geomagnetic field behavior. For more widely separated sites, however, their differences may depend on their proximity to the reversed flux that initiates the reversal.

The VGP paths during the MBT from the Leonhardt and Fabian (2007) reconstruction also show differences between northern and southern hemispheres related to differences in reverse flux generation. According to their reconstruction, the final MBT reversal begins with reverse flux emerging across the CMB beneath the north Pacific, starting around 783 ka, nearly 11 kyr before their dipole minimum shown in Fig. 6c. Their analysis of VGP paths yields a reversal age defined by the VGP equator crossing around 781 ka for north Pacific sites, compared to around 772 ka for sites in the south Atlantic, a difference of nearly 9 kyr. Much of this difference is attributable to the delayed appearance of reversed flux in the southern hemisphere in their reconstruction. Similarly, their model VGP paths from high northern latitude sites, especially sites in the north Pacific, show early onset of directional instability and increased path complexity, compared to VGPs from sites more distant from the origin point of the reversed field, an effect that is consistent with the behavior of our model reversal, except that our reversal begins in the south. Any differences that stem from the fact that the MBT was an R–N reversal (that evidently originated in the northern hemisphere) whereas our model reversal is N–R (and originates in the southern hemisphere) should not be given much significance, however, because our model equations and boundary conditions are symmetric across the model equator and our reversal could equally likely have been R–N and originated in the north.

4. Summary and discussion

Polarity reversals we have investigated are related to a transitional region in the parameter space that connects stable dynamos with axial dipole-dominated magnetic fields (at relatively low Ekman and Rayleigh numbers) to dynamos with highly variable fields in which the axial dipole is weak and unstable (at higher Ekman and Rayleigh numbers). We find that complex polarity reversals sometimes occur in this transitional region. The first stage in the reversal process is a dipole strength reduction, leading to the multi-polar field structure on the core–mantle boundary, which is sometimes quite slow. For example, a polarity reversal in our most Earth-like dynamo is preceded by a 5-fold reduction in the dipole intensity on the core–mantle boundary that lasts more than 100 kyr. Next is the multi-polar stage, during which the dipole field sometimes undergoes a precursory reversal and then recovers intensity in its original polarity. The last stage is the final directional change and intensity recovery in

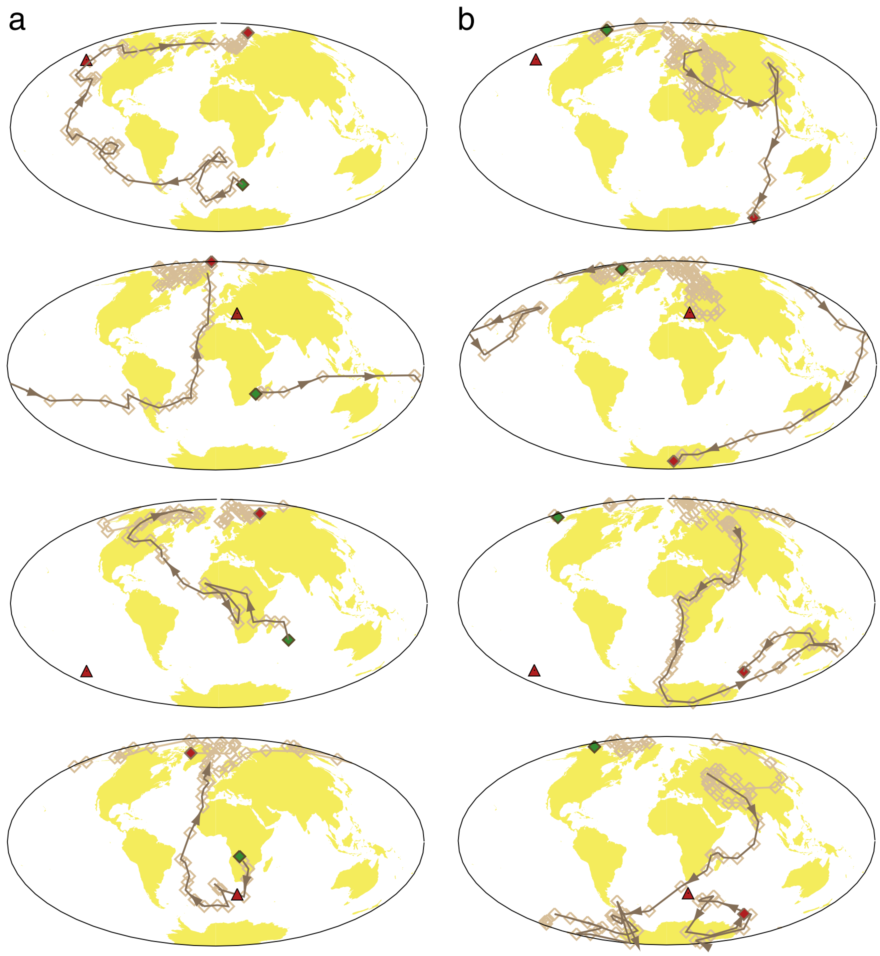

Fig. 8. VGP paths at sample locations during the polarity recovery and the final reversal in dynamo Case i. Left column (a) shows paths from sites at 45 N and 43 S starting at 2.84449 Myr and lasting 5.6 kyr including the polarity recovery; right column (b) shows paths from sites at 45 N and 43 S starting at 2.85485 Myr and lasting 8 kyr including the final polarity reversal. Large, late-stage directional changes are shown with arrows and darker paths. Continental outlines are shown for reference only, as the absolute longitudes are arbitrary. Data points are 95 years apart. Site locations are marked by triangles; first and last VGPs are colored in green and red, respectively.

the new polarity. We use the term complex reversal to describe the polarity events with this sequence.

The reversal mechanism in the case we analyzed initiates with the production and strengthening of reverse magnetic flux in the southern hemisphere of the core. As spots of the reverse flux strengthen and are transported beneath the core–mantle boundary, the dipole moment weakens in advance of the actual polarity change, marking the transition from stable dipolar to highly variable multi-polar states. In our model reversal, the directional transition is assisted by cross-equatorial meridional circulation. Sites close to the reversal origin record this complexity with early onset of directional instability and looping VGP paths. Sites distant from the reversal origin record a somewhat simpler, delayed transition with more north–south, longitude-confined VGP paths. This overall behavior is qualitatively consistent with reconstructions of the Matuyama–Brunhes polarity transition, although that transition was R–N and the evidence indicates it began in the north.

During stable polarity times, the antisymmetric part of the field on the core–mantle boundary (the dipole family) exceeds the symmetric part of the field (the quadrupole family) in our model. During transition field times, these two parts of the core–mantle boundary field become nearly the same in magnitude, mostly through the reduction in the dipole family strength. At the Earth's surface, the energy in the dipole and the non-dipole fields both decrease prior to the reversal, but the dipole energy decreases faster. During the multipolar stage the two energies are generally comparable, with the dipole energy occasionally falling below the non-dipole energy, especially at times of fast directional change. The lowest surface magnetic energies are found during these times, although greatly reduced surface magnetic energy persists for several thousand years following the reversal.

Although our findings are based on highly idealized numerical dynamos extrapolated to core conditions, they nevertheless suggest possible environmental consequences associated with complex geomagnetic reversals. During stable polarity times, the flux of high energy of particles (cosmic radiation) entering the Earth's upper and middle atmosphere is greatly reduced by the shielding effects of the strong, mostly dipolar external geomagnetic field. During polarity reversals and excursions, and for some time afterward, the efficiency of magnetospheric shielding is certainly far lower than normal, according to our results. Although the Earth's atmosphere normally shields the surface environment from cosmic radiation, during weak field times it is possible for high energy particles to access the upper atmosphere at most or all latitudes (Glassmeier et al., 2009) A number of models of the paleomagnetosphere have been constructed for idealized, hypothetical transition field geometries, including equatorial dipole structures and also quadrupoles (Vogt et al., 2004, 2007;

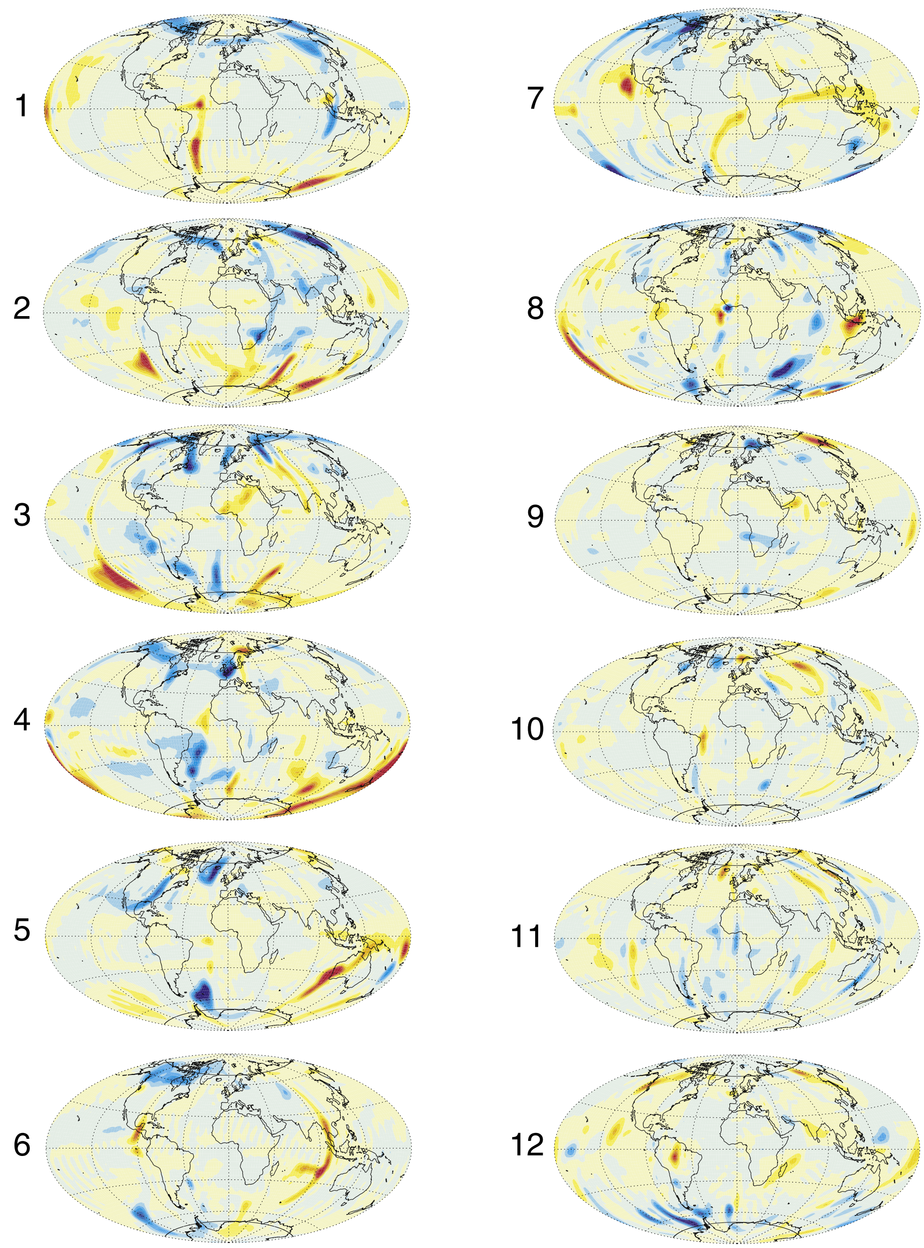

Fig. 9. Snapshots of the radial component of the magnetic field on the core–mantle boundary at 950 year intervals during the final polarity reversal in dynamo Case i, at times labeled 1–12 in Fig. 6. Red, blue = positive, negative radial field, respectively. Continental outlines are shown for reference only, as the absolute longitudes are arbitrary.

Zieger et al., 2004). The calculated environmental impact of the weak field states grows with time, and according to the above studies, also tends to increase with the harmonic content of the field structure. On this basis, one could speculate that environmental impact would be maximized during a complex reversal of the type described here, by virtue of its relatively long-lasting, low intensity, and sometimes multi-polar external field.

Acknowledgments

We gratefully acknowledge the support from CSEDI Grants 0652568, 0652370, and 0652423 from the National Science Foundation. Computing resources were provided by the High End Computing Program at NASA Ames, by the NSF at the Texas Advanced Computing Center and by an NSF supported cluster at the University of California, Santa Cruz. We thank Paul Roberts and Hagay Amit for stimulating discussions on reversals, as well as Roman Leonhardt and Karl Fabian for sharing their MBT reconstruction.

References

Amit, H., Leonhardt, R., Wicht, J., 2011. Polarity reversals from paleomagnetic observations and numerical dynamo simulations. Space Sci. Rev. 155, 293–355.
Aubert, J., Aurnou, J., Wicht, J., 2008. The magnetic structure of convection-driven numerical dynamos. Geophys. J. Int. 172, 945–956.
Berhanu, M., Monchaux, R., Fauve, S., et al., 2007. Magnetic field reversals in an experimental turbulent dynamo. Europhys. Lett. 77, 59001.
Braginsky, S., Roberts, P., 1995. Equations governing convection in Earth's core and the geodynamo. Geophys. Astrophys. Fluid Dyn. 79, 1–97.
Channell, J.E.T., Lehman, B., 1997. The last two geomagnetic polarity reversals recorded in high-deposition-rate-sediment drifts. Nature 389, 712–715.
Christensen, U., Aubert, J., 2006. Scaling properties of convection-driven dynamos in rotating spherical shells and application to planetary fields. Geophys. J. Int. 166, 97–114.
Clement, B.M., 1991. Geographical distribution of transitional VGPs — evidence for non-zonal equatorial symmetry during the Matuyama–Brunhes geomagnetic reversal. Earth Planet. Sci. Lett. 104, 48–58.

Clement, B.M., 2004. Dependence of the duration of geomagnetic polarity reversals on site latitude. Nature 428, 637–640.
Clement, B.M., Kent, D.V., 1987. Geomagnetic polarity transition records from 5 hydraulic piston core sites in the North Atlantic. Deep Sea Drilling Project, Initial Rep, 94, p. 831852.
Coe, R.S., Glatzmaier, G.A., 2006. Symmetry and stability of the geomagnetic field. Geophys. Res. Lett. 33, L21311.
Coe, R.S., Glen, J.M.G., 2004. The Complexity of Reversals, in Geophysical Monograph Series 145: Timescales of the Internal Geomagnetic Field. In: Channell, J.E.T., Kent, D.V., Lowrie, W., Meert, J.G. (Eds.), American Geophysical Union, Washington DC, pp. 221–232.
Coe, R.S., Hongre, L., Glatzmaier, G.A., 2000. An examination of simulated geomagnetic reversals from a palaeomagnetic perspective. Philos. Trans. R. Soc. Lond. A358, 1141–1170.
Driscoll, P., Olson, P., 2009. Effects of buoyancy and rotation on the polarity reversal frequency of gravitationally-driven numerical dynamos. Geophys. J. Int. doi:10.111/j.1365-246X.2009.04234.x.
Glassmeier, K.H., Richter, O., Vogt, J., Mobus, P., Schwalb, A., 2009. The sun, geomagnetic polarity transitions, and possible biospheric effects: review and illustrating model. Int. J. Astrobiol. 8, 147–159.
Glatzmaier, G.A., 1984. Numerical simulations of stellar convective dynamos I. The model method. J. Comp. Phys. 55, 461–484.
Glatzmaier, G.A., Coe, R.S., 2007. Magnetic reversals in the core. In: Olson, P. (Ed.), Treatise on Geophysics, vol. 8. Elsevier B.V., pp. 283–299.
Glatzmaier, G.A., Roberts, P.H., 1995. A three-dimensional self-consistent computer simulation of a geomagnetic field reversal. Nature 377, 203–209.
Glatzmaier, G.A., Roberts, P.H., 1996. An anelastic evolutionary geodynamo simulation driven by compositional and thermal convection. Physica D 97, 81–94.
Glatzmaier, G.A., Coe, R.S., Hongre, L., Roberts, P.H., 1999. The role of the Earth's mantle in controlling the frequency of geomagnetic reversals. Nature 401, 885–890.
Gubbins, D., 1999. The distinction between geomagnetic excursions and reversals. Geophys. J. Int. 137, 1–4.
Hartl, P., Tauxe, L., 1996. A precursor to the Matuyama/Brunhes transition-field instability as recorded in pelagic sediments. Earth Planet. Sci. Lett. 138, 121–135.
Hoffman, K.A., 1992. Dipolar reversal states of the geomagnetic field and core mantle dynamics. Nature 359, 789–794.
Hoffman, K.A., 1996. Transitional paleomagnetic field behavior: preferred paths or patches? Surv. Geophys. 17, 207211.
Ingham, M., Turner, G., 2008. Behaviour of the geomagnetic field during the Matuyama–Brunhes polarity transition. Phys. Earth Planet. Inter. 168, 163–178.
Kutzner, C., Christensen, U.R., 2002. From stable dipolar to reversing numerical dynamos. Phys. Earth Planet. Inter. 131, 29–45.
Kutzner, C., Christensen, U.R., 2004. Simulated geomagnetic reversals and preferred virtual geomagnetic pole paths. Geophys. J. Int. 157, 1105–1118.
Leonhardt, R., Fabian, K., 2007. Paleomagnetic reconstruction of the global geomagnetic field evolution during the Matuyama/Brunhes transition: iterative Bayesian inversion and independent verification. Earth Planet. Sci. Lett. 253, 172–195.
Leonhardt, R., McWilliams, M., Heider, F., Soffel, H.C., 2009. The Gilsa excursion and the Matuyama/Brunhes transition recorded in 40Ar/39Ar dated lavas from Lanai and Maui, Hawaiian Islands. Geophys. J. Int. 179, 4358.
Love, J.J., Mazaud, A., 1997. A database for the Matuyama–Brunhes magnetic reversal. Phys. Earth Planet. Int. 103, 207–245.
Monchaux, R., Berhanu, M., Bourgoin, M., et al., 2007. Generation of a Magnetic Field by Dynamo Action in a Turbulent Flow of Liquid Sodium. Phys. Rev. Lett. 98, 044502.
Olson, P., Christensen, U.R., 2006. Dipole moment scaling for convection-driven planetary dynamos. Earth Planet. Sci. Lett. 250, 561–571.
Olson, P., Driscoll, P., Amit, H., 2009. Dipole collapse and reversal precursors in a numerical dynamo. Phys. Earth Planet. Inter. 173, 121–140.
Olson, P.L., Coe, R.S., Driscoll, P.E., Glatzmaier, G.A., Roberts, P.H., 2010. Geodynamo Reversal Frequency and Heterogeneous Core–Mantle Boundary Heat Flow. Phys. Earth Planet. Inter. 180, 66–79. doi:10.1016/j.pepi.2010.02.010.
Rotvig, J., 2009. An investigation of reversing numerical dynamos driven by either differential or volumetric heating. Phys. Earth Planet. Int. 176, 69–82.
Singer, B.S., Hoffman, K.A., Coe, R.S., et al., 2005. Structural and temporal requirements for geomagnetic field reversal deduced from lava flows. Nature 434, 633–636.
Sorriso-Valvo, L., Carbone, V., Bourgoin, M., Odier, P., Plihon, N., Volk, R., 2009. Statistical analysis of magnetic field reversals in laboratory dynamo and in paleomagnetic measurements. Int. J. Mod. Phys. B 23, 5483–5491.
Takahashi, F., Matsushima, M., Honkura, Y., 2005. Simulations of a quasi-Taylor state geomagnetic field including polarity reversals on the earth simulator. Science 309, 459–461.
Takahashi, F., Matsushima, M., Honkura, Y., 2007. A numerical study on magnetic polarity transition in an MHD dynamo model. Earth Planet. Space 59, 665–673.
Valet, J.P., Meynadier, L., Guyodo, Y., 2005. Geomagnetic dipole strength and reversal rate over the past two million years. Nature 435, 802–805.
Valet, J.-P., Plenier, G., Herrero-Bervera, E., 2008. Geomagnetic excursions reflect an aborted polarity state. Earth Planet. Sci. Lett. 274, 472–478.
Vogt, J., Zieger, B., Glassmeier, K.-H., Stadelmann, A., Gombosi, T., Hansen, K.C., Ridley, A., 2004. MHD simulations of quadrupolar paleomagnetospheres. J. Geophys. Res. 109, A12221. doi:10.1029/2003JA010273.
Vogt, J., Zieger, B., Glassmeier, K.-H., Stadelmann, A., Kallenrode, M.-B., Sinnhuber, M., Winkler, H., 2007. Energetic particles in the paleomagnetosphere: reduced dipole configurations and quadrupolar contributions. J. Geophys. Res. 112, A06216 doi:117810.1029/2006JA012224.
Wicht, J., 2005. Palaeomagnetic interpretation of dynamo simulations. Geophys. J. Int. 162 (1180), 371–380.
Wicht, J., Olson, P., 2004. A detailed study of the polarity reversal mechanism in a numerical dynamo model. Geochem. Geophys. Geosyst. 5 (Q03H10), 1–23.
Wicht, J., Stellmach, S., Harder, H., 2009. Numerical models of the geodynamo: from fundamental Cartesian models to 3D simulations of field reversals. In: Glassmeier, K., Soffel, H., Negendank, J. (Eds.), Geomagnetic Field Variations: Space-Time Structure, Processes, and Effects on System Earth. Springer Berlin.
Zieger, B., Vogt, J., Glassmeier, K.H., Gombosi, T., 2004. Magnetohydrodynamic simulation of an equatorial dipolar paleomagnetosphere. J. Geophys. Res. 109, A07205. doi:10.1029/2004JA010434.